J. Fluid Mech. (2001), *vol.* 430, *pp.* 87–109. Printed in the United Kingdom

Turbulent energy scale budget equations in a fully developed channel flow

By L. DANAILA[1]†, F. ANSELMET[1], T. ZHOU[2] AND R. A. ANTONIA[2]

[1]IRPHE, 12 Avenue Général Leclerc, 13003 Marseille, France

[2] Department of Mechanical Engineering, University of Newcastle, NSW, 2308, Australia

(Received 20 April 2000 and in revised form 25 August 2000)

Kolmogorov's equation, which relates second- and third-order moments of the velocity increment, provides a simple method for estimating the mean energy dissipation rate $\langle\epsilon\rangle$ for homogeneous and isotropic turbulence. However, this equation is usually not verified in small to moderate Reynolds number flows. This is due partly to the lack of isotropy in either sheared or non-sheared flows, and, more importantly, to the influence, which is flow specific, of the inhomogeneous and anisotropic large scales. These shortcomings are examined in the context of the central region of a turbulent channel flow. In this case, we propose a generalized form of Kolmogorov's equation, which includes some additional terms reflecting the large-scale turbulent diffusion acting from the walls through to the centreline of the channel. For moderate Reynolds numbers, the mean turbulent energy transferred at a scale r also contains a large-scale contribution, reflecting the non-homogeneity of these scales. There is reasonable agreement between the new equation and hot-wire measurements in the central region of a fully developed channel flow.

1. Introduction

Kolmogorov's equation can be derived from the Navier–Stokes equations, using homogeneity and isotropy:

$$-\langle(\Delta u_1)^3\rangle + 6\nu\frac{\mathrm{d}}{\mathrm{d}r}\langle(\Delta u_1)^2\rangle = \tfrac{4}{5}\langle\epsilon\rangle r, \tag{1.1}$$

with the increment $\Delta u_1(r) \equiv u_1(x_1+r)-u_1(x_1)$, where u_1 is the longitudinal (streamwise) velocity component, and $\langle\epsilon\rangle$ is the mean energy dissipation rate:

$$\langle\epsilon\rangle = \frac{1}{2}\nu\left\langle\left(\frac{\partial u_i}{\partial x_j}+\frac{\partial u_j}{\partial x_i}\right)^2\right\rangle. \tag{1.2}$$

Here, repeated indices indicate summation, ν is the kinematic viscosity of the fluid, u_i is the fluctuating velocity component in the ith-direction, and angular brackets denote time averaging.

Equation (1.1) is of fundamental interest, since it is an equilibrium equation between second- and third-order moments; one interpretation is that it represents a mean turbulent energy balance for each scale r. Writing (1.1) as $A + B = C$, term C,

† Present address: LET, University of Poitiers, 40 Avenue du Recteur Pineau, 86022 Poitiers, France.

which is directly proportional to the dissipation rate $\langle\epsilon\rangle$, is associated with the energy transferred at any scale r. This equation indicates that the mean energy transferred at a scale r is made up of both the energy lost through the turbulent advection (term A) and the energy lost by molecular destruction (term B). It can be interpreted as an energy budget equation involving $\langle\epsilon\rangle$, but it can also be thought of as an equation which provides information about $\langle\epsilon\rangle$. The equation is a relatively simple means of obtaining $\langle\epsilon\rangle$, as the second- and third-order moments can be inferred from single hot-wire measurements via Taylor's hypothesis. Equation (1.1) is essentially a mean turbulent energy budget equation and does not contain high-order moments. In this form, it does not reflect the influence of small-scale (internal) intermittency. The implications of this equation in the context of internal intermittency will be discussed later. In order to determine how closely measurements satisfy (1.1), an accurate determination of $\langle\epsilon\rangle$ is required. This represents a major experimental challenge since all the derivatives in (1.2) need to be estimated. For statistically steady systems, $\langle\epsilon\rangle$ is identical to the rate of energy injected at the large scales, and obviously, the same as the rate of energy transferred at each scale through the cascade. This reflects the hybrid nature of $\langle\epsilon\rangle$, which is not just a small-scale quantity but also contains information about the energy which has been transferred from the large scales down to the small scales.

Since spatial derivatives of velocity fluctuations are very difficult to measure accurately, additional hypotheses are necessary. Homogeneity leads to $\langle\epsilon\rangle_{hom} \equiv \nu\langle(\partial u_i/\partial x_j)^2\rangle$, where generally the subscript indicates the method or hypothesis used to estimate $\langle\epsilon\rangle$, and the absence of a subscript signifies that the 'true' $\langle\epsilon\rangle$, given by (1.2), is referred to. A relatively crude approximation for $\langle\epsilon\rangle_{hom}$ is obtained by supposing that the three spatial directions are equivalent so that only derivatives with respect to x_1 appear in the expression, namely

$$\langle\epsilon\rangle_{hom} \equiv 3\nu\left\langle\left(\frac{\partial u_i}{\partial x_1}\right)^2\right\rangle. \tag{1.3}$$

Local isotropy results in (Monin & Yaglom 1975)

$$\langle\epsilon\rangle_{iso} \equiv 15\nu\left\langle\left(\frac{\partial u_1}{\partial x_1}\right)^2\right\rangle. \tag{1.4}$$

Equation (1.4) is the simplest and most often used relation for obtaining the mean turbulent energy dissipation rate. Its ability to provide a good approximation to the 'true' value of $\langle\epsilon\rangle$ hinges on whether the small-scale motion is isotropic. It is also worth emphasizing that the quality of the data and data processing are important. Here we recall the errors caused by the finite spatial resolution of the probe, and the need to apply (spectral) corrections before a 'correct' value of $\langle\epsilon\rangle_{iso}$ can be obtained. To bypass these difficulties, a simpler way of estimating $\langle\epsilon\rangle$ is to focus on the larger scales of the flow. There is thus a strong incentive to devise a method for inferring $\langle\epsilon\rangle$ which eliminates the need to evaluate velocity derivatives.

The inertial range (IR) is defined as the range of scales which are much smaller than the injection scale, and much larger than the dissipative scale (comparable to the Kolmogorov length scale $\eta \equiv (\nu^3/\langle\epsilon\rangle)^{1/4}$). In the IR, (1.1) reduces to

$$-\langle(\Delta u_1)^3\rangle = \tfrac{4}{5}\langle\epsilon\rangle r. \tag{1.5}$$

Equation (1.5) could be used as a practical method to obtain $\langle\epsilon\rangle$, since a single hot-wire measurement yields $\langle(\Delta u_1)^3\rangle$ (Anselmet *et al.* 1984). In practice, $\langle\epsilon\rangle$ is inferred

from the so-called 'plateau' method, whereby the ratio $-\langle(\Delta u_1)^3\rangle/(4r/5)$ is plotted vs. r. A similar approach has been used in estimating $\langle\epsilon\rangle$ from the u_1-spectrum (e.g. Saddoughi 1997). It should be stressed that (1.5) is strictly valid only when the IR is established. This is expected only at very large Reynolds numbers (e.g. Qian 1997) or when the conditions of stationarity, isotropy and homogeneity are strictly satisfied. Equation (1.1) is verified only for small scales when the Taylor-microscale Reynolds number R_λ is moderate (Antonia, Chambers & Browne 1983, see also figure 3) ($R_\lambda \equiv u_1'\lambda/\nu$, where a prime denotes the r.m.s. value and $\lambda \equiv u_1'/(\partial u_1/\partial x_1)'$ is the longitudinal Taylor microscale). At larger scales, the approach to a four-fifths law is expected to be quite slow, as demonstrated by Qian (1999).

Using a Taylor series expansion about $r = 0$, equation (1.1) reduces to the isotropic form of $\langle\epsilon\rangle$:

$$\lim_{r\to 0} 6\nu\frac{\mathrm{d}}{\mathrm{d}r}\langle(\Delta u_1)^2\rangle = 6\nu\frac{\mathrm{d}}{\mathrm{d}r}\left[\left\langle\left(\frac{\partial u_1}{\partial x_1}\right)^2\right\rangle r^2\right] = 12\nu\left\langle\left(\frac{\partial u_1}{\partial x_1}\right)^2\right\rangle r = \tfrac{4}{5}\langle\epsilon\rangle r \quad \Rightarrow$$

$$\langle\epsilon\rangle = 15\nu\left\langle\left(\frac{\partial u_1}{\partial x_1}\right)^2\right\rangle = \langle\epsilon\rangle_{iso}. \qquad (1.6)$$

A more general relation between second- and third-order moments of velocity increments, namely

$$-\langle\Delta u_1(\Delta u_i)^2\rangle + 2\nu\frac{\mathrm{d}}{\mathrm{d}r}\langle(\Delta u_i)^2\rangle = \tfrac{4}{3}\langle\epsilon\rangle r \qquad (1.7)$$

was presented in Antonia *et al.* (1997*a*), where the analogy between (1.7) and Yaglom's equation for temperature increments was also discussed. Equation (1.7) actually represents an extended form (for all velocity components) of Kolmogorov's equation. It is consistent, for very small scales, with the homogeneous form of $\langle\epsilon\rangle$:

$$2\nu\lim_{r\to 0}\frac{\mathrm{d}}{\mathrm{d}r}\langle(\Delta u_i)^2\rangle = 4\nu\left\langle\left(\frac{\partial u_i}{\partial x_1}\right)^2\right\rangle r = \tfrac{4}{3}\langle\epsilon\rangle r \quad \Rightarrow$$

$$\langle\epsilon\rangle = 3\nu\left\langle\left(\frac{\partial u_i}{\partial x_1}\right)^2\right\rangle = \langle\epsilon\rangle_{hom}. \qquad (1.8)$$

Equations (1.1) and (1.7) characterize the energy equilibrium state of the flow for stationary isotropic turbulence. Our objective is to gain some insight into the physical significance of the imbalance between the left and right sides of (1.1), for moderate Reynolds numbers. It is reasonable to think that at least one term is needed to account for this imbalance. This term plays the role of a 'forcing' term, and its contribution would be mainly to re-establish the energy balance for the large scales.

Kolmogorov's equation with an additional forcing term was presented in a generic form by Frisch (1995) and re-discussed, in the wider context of local homogeneity and isotropy, by Hill (1997). A particular form for decaying turbulence was given by Saffman (1968). Lindborg (1999) analysed a generalized form of Kolmogorov's equation which takes into account a time-dependent term. This new term was further estimated using the $k-\epsilon$ model. The generalized equation was then tested against measurements in grid turbulence and on the axes of a jet and a wake. Reasonable agreement was obtained in each case. This is somewhat surprising in the context of the jet and the wake since the analysis neglected the large-scale lateral turbulent diffusion for these two flows.

Moisy, Tabeling & Willaime (1999) studied another model-containing form of Kolmogorov's equation, previously deduced by Novikov (1965). The supplementary term involves an external length scale, which characterizes the forcing in a global manner. Using measurements in low-temperature helium gas, they assumed the validity of the equation over a limited range of scales, approximately corresponding to the IR, and indirectly inferred the magnitude of the external length scale.

While the two previous studies involved modelling, a different approach was considered by Danaila *et al.* (1999). Generalized forms of Kolmogorov's and Yaglom's equations were written and tested in isothermal and non-isothermal decaying grid turbulence. No modelling was required, and the additional term was estimated directly from measurements. This new term reflects the non-stationarity (in a reference system moving with the mean stream) or the large-scale non-homogeneity along the stream direction, when using a fixed reference system. This generalized equation is an exact expression, although adequate for decaying grid turbulence only. The same supplementary term is unlikely to apply to other flows. As emphasized in Danaila *et al.* (1999), continuous energy injection flows, such as boundary layers and channel flows, differ from decaying flows, e.g. grid turbulence, jets and wakes.

In the present paper, we identify the origin of the imbalance between the different terms in (1.1) and (1.7) at the centreline of a fully developed channel flow for relatively small Reynolds numbers. There is no streamwise decay, but $\langle\epsilon\rangle$ must balance the lateral diffusion in the wall-normal direction x_3. Different generalized forms of Kolmogorov's equation, appropriate to this flow, are deduced in § 2. Accordingly, different estimations of $\langle\epsilon\rangle$ are critically compared in § 4 following a brief description of the experiment in § 3, and the generalized equations are compared with measurement in § 5. Another modification of the Kolmogorov equation, wherein the assumption of local homogeneity is relaxed further, is developed and compared with measurements in § 6.

2. Theoretical considerations

As noted earlier, the main objective is to gain some insight into the flow physics which results in an imbalance between the left- and right-hand sides of (1.1) on the channel centreline at small/moderate Reynolds numbers. The slight (large-scale) non-homogeneity, which causes this difference, is taken into account when deriving Kolmogorov's equation, although local isotropy is still used for all the other terms: turbulent advection, molecular diffusion, and pressure-containing terms. From a mathematical point of view, the extra non-homogeneous term is introduced and manipulated in a quasi-isotropic context. In order to highlight the manner in which this term comes about, we recall briefly the salient steps in the derivation of Kolmogorov's equation.

Using the same procedure as presented in Monin & Yaglom (1975, hereafter referred to as MY), we consider a fixed reference system $\mathscr{S}$ in which the coordinates and velocity components are $\boldsymbol{x}$ and $\boldsymbol{u}$, and a moving reference system for which the origin $\boldsymbol{x}^+$ moves with the velocity $\boldsymbol{u}^+$. We then write the incompressible Navier–Stokes equations at the two points $\boldsymbol{x}$ and $\boldsymbol{x}^+$, separated by the increment $\boldsymbol{r} = \boldsymbol{x}^+ - \boldsymbol{x}$:

$$\partial_t u_i + u_\alpha \partial_\alpha u_i = -\partial_i p/\rho + \nu \partial_\alpha^2 u_i, \tag{2.1}$$

$$\partial_t u_i^+ + u_\alpha^+ \partial_\alpha^+ u_i^+ = -\partial_i^+ p^+/\rho + \nu \partial_\alpha^{2+} u_i^+. \tag{2.2}$$

The superscript + refers to $\boldsymbol{x}^+$, and ρ is the fluid density. In (2.1) and (2.2), u_i is the instantaneous velocity vector, with $\langle u_i\rangle = U_1\delta_{i1}$ (δ_{ij} is Kronecker's symbol, and U_1 is the mean velocity of the flow); p is the pressure, $\partial_t \equiv \partial/\partial t$, $\partial_\alpha \equiv \partial/\partial x_\alpha$ and ∂_α^2 is the

Laplacian $\partial^2/\partial x_\alpha^2$ (hereafter, the notation ∂_α and ∂_α^+ will be used to denote derivatives with respect to x_α and x_α^+; when other spatial variables are involved, the derivatives will be written explicitly, e.g. $\partial/\partial r$ or $\partial/\partial X_\alpha$). We then consider that the two points $\boldsymbol{x}$ and $\boldsymbol{x}^+$ are independent, i.e. u_i depends only on $\boldsymbol{x}$ and u_i^+ depends only on $\boldsymbol{x}^+$, so that subtraction of (2.1) from (2.2) yields an equation for the velocity increment $\Delta u_i = u_i^+ - u_i$:

$$\partial_t(\Delta u_i)+U_1\partial_1(\Delta u_i)+u_\alpha^+\partial_\alpha^+(\Delta u_i)+u_\alpha\partial_\alpha(\Delta u_i) = -(\partial_i+\partial_i^+)(\Delta p)/\rho+\nu(\partial_\alpha^2+\partial_\alpha^{2+})(\Delta u_i). \tag{2.3}$$

In (2.3) we explicitly used the mean velocity U_1, while, for simplicity, u_i denotes the fluctuating velocity field, with $\langle u_i\rangle = 0$. Hereafter, u_i only denotes the fluctuating velocity.

By subtracting and adding the term $u_\alpha\partial_\alpha^+(\Delta u_i)$ to the left-hand side of (2.3),

$$\partial_t(\Delta u_i) + U_1\partial_1(\Delta u_i) + \Delta(u_\alpha)\partial_\alpha^+(\Delta u_i) + u_\alpha\partial_\alpha^+(\Delta u_i) + u_\alpha\partial_\alpha(\Delta u_i) = -(\partial_i + \partial_i^+)(\Delta p)/\rho + \nu(\partial_\alpha^2 + \partial_\alpha^{2+})(\Delta u_i). \tag{2.4}$$

Assuming local homogeneity, all derivatives with respect to different spatial directions can be written using the components of $\boldsymbol{r}$ (Hill 1997, or Antonia *et al.* 1997*a*)

$$\partial_i^+ \equiv \frac{\partial}{\partial r_i}, \quad \partial_i \equiv -\frac{\partial}{\partial r_i}. \tag{2.5}$$

Equation (2.4) becomes

$$(\partial_t + U_1\partial_1)(\Delta u_i) + \Delta(u_\alpha)\frac{\partial(\Delta u_i)}{\partial r_\alpha} + u_\alpha[\partial_\alpha^+ + \partial_\alpha](\Delta u_i) = -(\partial_i + \partial_i^+)(\Delta p)/\rho + \nu(\partial_\alpha^2 + \partial_\alpha^{2+})(\Delta u_i). \tag{2.6}$$

As already emphasized in Antonia *et al.* (1997*a*), the third term on the left is omitted in the derivation of the same equation in MY. This disagreement arises from the use of different reference systems: MY used a translating reference system for the left-hand side of the equation, but the right-hand side was written in a fixed reference system (see (22.14) in MY). A fixed reference system ($\mathscr{S}$) has been used consistently in (2.6). The third term on the left of (2.6) will be retained and we will show that it is important when considering slightly non-homogeneous flows, such as the channel flow.

In the first instance, we follow the same procedure as in MY (p. 401), but retaining the new term on the left of (2.6). The evolution equation for the mixed structure function $D_{ij}(\boldsymbol{r}) = \langle\Delta u_i\Delta u_j\rangle(\boldsymbol{r})$ can be obtained by first multiplying both sides of (2.6) by Δu_j, and both sides of the analogous equation (for the increment Δu_j) by Δu_i, then adding the two equations and averaging:

$$(\partial_t + U_1\partial_1)D_{ij}(\boldsymbol{r}) + \langle u_\alpha[\partial_\alpha + \partial_\alpha^+](\Delta u_i\Delta u_j)\rangle(\boldsymbol{r}) + \frac{\partial D_{ijk}}{\partial r_k}(\boldsymbol{r}) = 2\nu\partial_\alpha^2 D_{ij}(\boldsymbol{r}) - \tfrac{4}{3}\langle\epsilon\rangle\delta_{ij}, \tag{2.7}$$

where $D_{ijk}(\boldsymbol{r}) = \langle\Delta u_i\Delta u_j\Delta u_k\rangle(\boldsymbol{r})$ is the third-order mixed structure function, and $\langle\epsilon\rangle = \langle\epsilon\rangle_{hom}$. The first two terms are specific to our work, while the others can be found in e.g. (22.15) of MY. This derivation assumes however some 'classical' Kolmogorov-like hypotheses: local homogeneity and local isotropy of the flow, and large turbulent Reynolds numbers. Local isotropy also leads to the vanishing of all terms containing pressure correlations (see MY, or Antonia *et al.* 1997*a*). Since the present focus is on the centreline of the channel flow, the local isotropy assumption seems reasonable (e.g. Antonia, Kim & Browne 1991), at least for some of the terms. Had the focus been

on the flow region away from the centreline, local isotropy would not be adequate, and pressure terms should be retained.

Note that, in a fixed reference system, the non-stationary term (∂_t) is zero, while the large-scale non-homogeneous term $U_1\partial_1$ only must be kept in decaying flows such as grid turbulence, jets and wakes. A fully developed turbulent channel flow does not decay with respect to x_1, so the first term $(\partial_t + U_1\partial_1)D_{ij}(\boldsymbol{r})$ is zero. More importantly, the second term on the left of (2.7) is specific to the present flow, and could be further written, using incompressibility and independence of $\boldsymbol{x}$ and $\boldsymbol{x}^+$, as

$$NH_{ij}(\boldsymbol{r}) = \langle u_\alpha[\partial_\alpha + \partial^+_\alpha](\Delta u_i \Delta u_j)\rangle(\boldsymbol{r}) \equiv [\partial_\alpha + \partial^+_\alpha]\langle u_\alpha \Delta u_i \Delta u_j\rangle(\boldsymbol{r}). \tag{2.8}$$

Homogeneity of the flow usually translates to $\partial_i\langle\ \rangle \equiv 0$ (see Hill 1997). The same identity holds when analysing relatively small scales of a locally homogeneous flow. In the channel flow, a slight large-scale non-homogeneity is to be taken into account, since statistical averages are not constant along the direction x_3 normal to the wall. Briefly,

$$\partial_1\langle\ \rangle = \partial_2\langle\ \rangle \equiv 0, \quad \partial_3\langle\ \rangle \neq 0, \tag{2.9}$$

and $NH_{ij}(\boldsymbol{r})$ can be finally written as

$$NH_{ij}(\boldsymbol{r}) = [\partial_3 + \partial^+_3]\langle u_3 \Delta u_i \Delta u_j\rangle(\boldsymbol{r}). \tag{2.10}$$

Note here that relation (2.9) applies to coordinates in a fixed reference system $\mathscr{S}$, in which x_3 is normal to the channel wall. We have adopted here a non-orthodox treatment of different terms in (2.7). NH_{ij} takes into account a small non-homogeneity at large scales, while all the other terms are based on local homogeneity and local isotropy. Hill (1997, p. 71) discussed in detail this aspect, noting that local homogeneity implies that 'statistics of derivatives present a very rapid variation with respect to $\boldsymbol{r}$ relative to the variation with respect to $\boldsymbol{X} \equiv (\boldsymbol{x} + \boldsymbol{x}^+)/2$, provided that $\boldsymbol{r}$ is sufficiently small ... when derivatives with respect to $\boldsymbol{x}$ or $\boldsymbol{x}^+$ are transformed into derivatives with respect to $\boldsymbol{r}$ and $\boldsymbol{X}$, the differentiation with respect to $\boldsymbol{X}$ being negligible compared to that with respect to $\boldsymbol{r}$'. This rule has been applied when evaluating the nonlinear term $\partial D_{ijk}/\partial r_k$.

The approach used in deriving the 'classical' Kolmogorov equation consists of contracting all tensors in (2.7), i.e. taking the sum of all terms in this equation, with respect to the indices $i = j$. Since terms such as the turbulent advection and molecular diffusion are rather small-scale phenomena, they could be then considered as being locally isotropic, and could be treated in the same way as in the classical approach. We now consider physical and mathematical properties of the second-order non-homogeneous tensor $NH_{ij}(\boldsymbol{r})$, when the argument $\boldsymbol{r}$ is a vector oriented in any direction. This is an anisotropic tensor, since it explicitly contains a derivative and a velocity component along the x_3-direction. If the flow were isotropic, a replacement of the x_3-derivative by a derivative with respect to x_1 should lead to equivalent results. We will show that $NH_{ij}(\boldsymbol{r})$ exhibits properties similar to those of an isotropic second-order tensor, after using the fact that $\partial^+_3\langle\cdot\rangle = \partial_3\langle\cdot\rangle$, when the first quantity is estimated in a fixed reference system $\mathscr{S}$. In particular, we show in Appendix A that the properties of $NH_{ij}(\boldsymbol{r})$ are similar to those of $D_{ij}(\boldsymbol{r})$, which is reasonably isotropic on the channel centreline. The structure functions $D_{ij}(\boldsymbol{r})$ and $NH_{ij}(\boldsymbol{r})$ can both be expressed in terms of the longitudinal structure functions (depending only on separations along any spatial direction, e.g. x_1), via similar relations

$$D_{33}(r) = D_{11}(r) + \frac{r}{2}\frac{\mathrm{d}}{\mathrm{d}r}D_{11}(r), \tag{2.11}$$

and

$$NH_{33}(r) = NH_{11}(r) + \frac{r}{2}\frac{\mathrm{d}}{\mathrm{d}r}NH_{11}(r). \tag{2.12}$$

Relations (2.11) and (2.12) will be tested against experimental data in § 5. In this section, we have implicitly assumed that, if second-order structure functions (or correlations) are locally isotropic, then the new structure functions we have introduced also exhibit some quasi-isotropic properties, e.g. (2.12).

Local isotropy and projection onto the x_1-direction lead to the classical form of the Kolmogorov equation, except that the supplementary term $NH_{ij}(\boldsymbol{r})$ is retained. We have assumed local isotropy for all the classical terms, and that $NH_{ij}(\boldsymbol{r})$ has the same properties as $D_{ij}(\boldsymbol{r})$. Since the latter tensor can be written in terms of $D_{11}(r)$ (with r along x_1), the extra non-homogeneous tensor $NH_{ij}(\boldsymbol{r})$ is also written using $NH_{11}(r)$. Thus, the generalized form of the Kolmogorov equation is

$$-\langle(\Delta u_1)^3\rangle + 6\nu\frac{\mathrm{d}}{\mathrm{d}r}\langle(\Delta u_1)^2\rangle + \frac{6}{r^4}\int_0^r y^4[-\partial_3\langle u_3(\Delta u_1)^2\rangle(y)]\mathrm{d}y = \tfrac{4}{5}\langle\epsilon\rangle r, \tag{2.13}$$

where $r = |\boldsymbol{r}|$ is along x_1. The term containing the integral reflects the slight non-homogeneity of the flow since it contains derivatives with respect to x_3. We now consider the behaviour of (2.13) when $r \to \infty$ or, in practice, when r exceeds L, the integral length scale. As will be shown in § 5, the third term on the left is, like the second term, always positive so that $-\langle(\Delta u_1)^3\rangle$ will always be smaller than $(4/5)\langle\epsilon\rangle r$. The same result has already been obtained for decaying grid turbulence. The first and second terms on the left of (2.13) vanish, while the new non-homogeneous term (hereafter called NH) balances term C, which is proportional to $\langle\epsilon\rangle$. Since $\lim_{r\to\infty}\langle u_3(\Delta u_1)^2\rangle = \langle u_3 u_1^2\rangle$ (recall that $\boldsymbol{x}$ and $\boldsymbol{x}^+$ are independent), it follows that

$$\begin{aligned}\lim_{r\to\infty} NH &= \lim_{r\to\infty}\frac{6}{r^4}\int_0^r y^4[-\partial_3\langle u_3(\Delta u_1)^2\rangle]\mathrm{d}y \\ &= \frac{6}{L^4}\int_0^L y^4[-\partial_3\langle u_3(\Delta u_1)^2\rangle]\mathrm{d}y + \lim_{r\to\infty}\frac{6}{r^4}\int_L^r y^4[-\partial_3\langle u_3(\Delta u_1)^2\rangle]\mathrm{d}y.\end{aligned} \tag{2.14}$$

For $r > L$, all moments become independent of r. Thus, when $r \to \infty$,

$$6/L^4\int_0^L y^4[-\partial_3\langle u_3(\Delta u_1)^2\rangle]\mathrm{d}y \lll \lim_{r\to\infty}(6/r^4)\int_L^r y^4[-\partial_3\langle u_3(\Delta u_1)^2\rangle]\mathrm{d}y.$$

Then, using the large-scale limits of the mixed moments $\langle u_3(\Delta u_1)^2\rangle$

$$\lim_{r\to\infty} NH = \lim_{r\to\infty}\frac{6}{r^4}\int_L^r y^4[-\partial_3\langle u_3(\Delta u_1)^2\rangle]\mathrm{d}y = -\tfrac{6r}{5}\partial_3\langle u_3 u_1^2\rangle = \tfrac{4}{5}\langle\epsilon\rangle r, \tag{2.15}$$

or

$$\langle\epsilon\rangle = -\tfrac{3}{2}\partial_3\langle u_3 u_1^2\rangle. \tag{2.16}$$

Equation (2.16) can be perceived as a means of defining the mean energy dissipation rate (Townsend 1976), in the specific context of the centreline of a plane channel flow. A turbulent kinetic energy balance can be derived (e.g. equation (5.4.1) of Townsend 1976) from the Navier–Stokes equations

$$\begin{aligned}\tfrac{1}{2}\partial t\langle u_i^2\rangle + \tfrac{1}{2}\partial_j\langle u_j u_i^2\rangle &= -\partial_i\langle p u_i\rangle/\rho + \nu\langle u_i\partial_j^2 u_i\rangle \\ &= -\partial_i\langle p u_i\rangle/\rho + \tfrac{1}{2}\nu\partial_j^2\langle u_i^2\rangle - \langle\epsilon\rangle_{hom}.\end{aligned} \tag{2.17}$$

Using stationarity, $\partial_t\langle u_i^2\rangle \equiv 0$, while $\partial_j\langle u_j u_i^2\rangle = \partial_3\langle u_3 u_i^2\rangle$. Then, (2.17) becomes

$$\langle\epsilon\rangle_{hom} = -\tfrac{1}{2}\partial_3\langle u_3 u_i^2\rangle - \partial_3\langle p u_3\rangle/\rho + \tfrac{1}{2}\nu\partial_j^2\langle u_i^2\rangle, \tag{2.18}$$

where the first term on the right represents the u_3 diffusion, the second is the pressure diffusion, and the third is the viscous diffusion. Assuming isotropy, the correlation between pressure and velocity is zero (Laufer 1954). Other terms are simplified and written in terms of only one velocity component (u_1), the viscous–diffusion term is negligible sufficiently away from the wall. Equation (2.18) reduces to

$$\langle\epsilon\rangle_{iso}^{LS} \equiv -\tfrac{3}{2}\partial_3\langle u_3 u_1^2\rangle. \tag{2.19}$$

The subscript *iso* indicates that isotropy is assumed, while the superscript *LS* refers to large-scales and therefore to the fact that the one-point turbulent energy budget has been used for obtaining this relatively simple approximation to $\langle\epsilon\rangle$. Equation (2.16) clearly demonstrates that our generalization of the Kolmogorov equation is consistent, for very large scales, with the approximation $\langle\epsilon\rangle \simeq \langle\epsilon\rangle_{iso}^{LS}$. The degree to which measurements satisfy (2.16) will be discussed in § 5.

It is also possible to generalize (1.7), starting from (2.6). The procedure is the same as that presented in Antonia *et al.* (1997*a*). After multiplying this equation by $2\Delta u_i$, averaging, and using $4\langle\Delta u_i\partial_\alpha^2\Delta u_i\rangle = 2\langle\partial_\alpha^2(\Delta u_i)^2\rangle - 4\langle(\partial_\alpha u_i)^2\rangle$, we obtain

$$\begin{aligned}(\partial_t + U_1\partial_1)\langle(\Delta u_i)^2\rangle(\boldsymbol{r}) + \frac{\partial}{\partial r_\alpha}\langle\Delta u_\alpha(\Delta u_i)^2\rangle(\boldsymbol{r}) + [\partial_3 + \partial_3^+]\langle u_3(\Delta u_i)^2\rangle(\boldsymbol{r})\\ = 2\nu\frac{\partial^2}{\partial r_\alpha^2}\langle(\Delta u_i)^2\rangle(\boldsymbol{r}) - 4\nu\langle(\partial_\alpha u_i)^2\rangle - 2\langle\Delta u_i(\partial_i + \partial_i^+)\Delta p\rangle/\rho(\boldsymbol{r}).\end{aligned} \tag{2.20}$$

All statistical properties are constant with respect to x_1, except the mean pressure, which does not appear in our equations. Indeed, term $\Pi = \langle\Delta u_i(\partial_i + \partial_i^+)\Delta p\rangle$, which contains the pressure increment, could be written as

$$\Pi = \langle\Delta u_i(\partial_i + \partial_i^+)\Delta p\rangle \equiv 2\partial_3\langle\Delta u_3\Delta p\rangle,$$

since pressure increments are inferred from measurements at a single point x_1, via Taylor's hypothesis. Thus, the mean pressure does not directly enter term Π, at least to a first approximation. This term can be neglected on the centreline of a channel flow because the small scales are nearly isotropic there. For large separations, $\partial_3\langle\Delta u_3\Delta p\rangle \to 2\partial_3\langle u_3 p\rangle$, which is nearly zero on the channel centreline, because of local isotropy (see § 4). This is a relatively strong assumption since isotropy implies a zero correlation between pressure increments and velocity increments. Thus, $\langle\Delta u_3\Delta p\rangle$ is zero on the centreline, but not zero away from the centreline. The correlation between pressure increments and different statistical quantities needs further investigation, and term Π should not be negligible away from the centreline. With these simplifications, and $\nu\langle(\partial_\alpha u_i)^2\rangle = \langle\epsilon\rangle$, (2.20) reduces to

$$\begin{aligned}(\partial_t + U_1\partial_1)\langle(\Delta u_i)^2\rangle(\boldsymbol{r}) + \frac{\partial}{\partial r_\alpha}\langle\Delta u_\alpha(\Delta u_i)^2\rangle(\boldsymbol{r})\\ + [\partial_3 + \partial_3^+]\langle u_3(\Delta u_i)^2\rangle(\boldsymbol{r}) = 2\nu\frac{\partial^2}{\partial r_\alpha^2}\langle(\Delta u_i)^2\rangle(\boldsymbol{r}) - 4\langle\epsilon\rangle.\end{aligned} \tag{2.21}$$

After projecting (2.21) onto the x_1-direction, we invoke local isotropy for those terms which characterize dissipative and IR scales, i.e. $\langle(\Delta u_i)^2\rangle(\boldsymbol{r})$ and $\langle\Delta u_\alpha(\Delta u_i)^2\rangle(\boldsymbol{r})$. For local isotropy, these structure functions depend only on the modulus $r = |\boldsymbol{r}|$. We have previously shown that $\langle\Delta u_i\Delta u_j\rangle(\boldsymbol{r})$ and $\partial_3\langle u_3\Delta u_i\Delta u_j\rangle(\boldsymbol{r})$ have similar properties under

local isotropy, so their contractions are also analogous. If the first is isotropic and depends on r only, then the second also depends only on r. This does not imply that $NH_{ij}(\boldsymbol{r})$ is isotropic, since it explicitly contains a derivative with respect to x_3. We choose x_1 as the direction onto which the projection is implemented. For simplicity, we drop the index 1 in r_1, keeping in mind that, when performing an experiment, this separation is measured along x_1. Equation (2.21) becomes

$$(\partial_t + U_1\partial_1)\langle(\Delta u_i)^2\rangle(r) + \left(\frac{2}{r} + \frac{\partial}{\partial r}\right)\langle\Delta u_1(\Delta u_i)^2\rangle(r) + [\partial_3 + \partial_3^+]\langle u_3(\Delta u_i)^2\rangle(r) = 2\nu\left(\frac{2}{r} + \frac{\partial}{\partial r}\right)\frac{\partial}{\partial r}\langle(\Delta u_i)^2\rangle(r) - 4\langle\epsilon\rangle. \tag{2.22}$$

Using stationarity and streamwise homogeneity, (2.22) can be reduced to

$$-\langle\Delta u_1(\Delta u_i)^2\rangle + 2\nu\frac{\mathrm{d}}{\mathrm{d}r}\langle(\Delta u_i)^2\rangle + \frac{2}{r^2}\int_0^r y^2[-\partial_3\langle u_3(\Delta u_i)^2\rangle]\mathrm{d}y = \tfrac{4}{3}\langle\epsilon\rangle r, \tag{2.23}$$

where y is a dummy variable, identifiable with the separation along x_1. Equation (2.23) can be written in the dimensionless form

$$A + B + NH = C,$$

with $C = (4/3)r/\eta$. NH expresses the slight non-homogeneity of the flow and includes all velocity components. The limiting form, at very large scales, of this equation can be obtained by applying the same method used in connection with (2.14) and (2.15). The result is

$$\lim_{r\to\infty} NH = \lim_{r\to\infty}\frac{-2}{r^2}\int_L^r y^2\partial_3\langle u_3(\Delta u_i)^2\rangle\mathrm{d}y = -\tfrac{2r}{3}\partial_3\langle u_3 u_i^2\rangle = \tfrac{4}{3}\langle\epsilon\rangle r. \tag{2.24}$$

We now introduce another definition of $\langle\epsilon\rangle$, slightly more general than (2.19), which may be inferred from (2.18). This is a kinetic energy balance equation, using homogeneity and only weak isotropy (pressure diffusion is neglected):

$$\langle\epsilon\rangle_{hom}^{LS} = -\tfrac{1}{2}\partial_3\langle u_3 u_i^2\rangle, \tag{2.25}$$

where the subscript *hom* indicates that the strongest hypothesis used here is homogeneity, and the superscript *LS* indicates that it is a one-point approach, so that it concerns the large scales of the flow. Equation (2.24) then reduces to $\langle\epsilon\rangle = \langle\epsilon\rangle_{hom}^{LS}$. The generalized form of the extended Kolmogorov equation (2.23) is therefore consistent, at the very large scales, with the equality $\langle\epsilon\rangle = \langle\epsilon\rangle_{hom}^{LS}$.

3. Experimental conditions

The open-circuit type channel flow is supplied by a centrifugal blower driven by a 8.4 kW Siemens motor equipped with a thyristor speed controller. Two cylinders of 1.6 mm diameter were fixed on each of the main walls near the entrance of the channel to trip the boundary layers. The working section is 7.32 m long, 0.76 m high and 0.042 m wide. The aspect ratio (≈ 18) is sufficiently large for the mean flow to be approximately two-dimensional. The measurements were made at a Reynolds number $Re = 3300$ ($Re \equiv U_0 h/\nu$, where $U_0 \equiv 2.5\,\mathrm{m\,s^{-1}}$ is the mean velocity at the centreline and h is the channel half-width). On the centreline, the Taylor-microscale Reynolds number R_λ is about 36, and the Kolmogorov length scale η, based on the mean energy dissipation rate $\langle\epsilon\rangle_{iso}$, is about 0.5 mm. The measurement location was at $340h$ from

the entrance. The measured mean static pressure gradient and moments of u_1 and u_3 along the centreline indicated that the flow was fully developed at $x_1 \simeq 150h$. Also note that, at the measurement location, the turbulence intensity u_1'/U_1 is about 4% and the ratio u_1'/u_2' about 1.25 on the centreline.

The data used in this paper were obtained from the two inclined wires of a lateral vorticity probe. A detailed description of this probe is given in Zhou *et al.* (1998). The inclined wires allowed the determination of u_1 and u_3 fluctuations. The included angle of the two wires is about 100°. The separation between the wires was about 1.2 mm. The hot wires were etched from 2.5 μm diameter Wollaston Pt–10% Rh wires with an active length of about 0.5 mm. The length to diameter ratio of the wires was about 200. The probe was calibrated at the centreline of the channel against a Pitot tube connected to a MKS Baratron pressure transducer (least count = 0.01 mm water). The yaw calibration was performed over $\pm 24°$ (using 4° steps). For each angle, the probe was relocated at the centreline of the channel. The probe was traversed in the x_3-direction between about 1 mm from the wall to 2 mm beyond the centreline.

The hot wires were operated with constant-temperature anemometers at an overheat ratio of 1.5. The output signals from the anemometers were passed through buck and gain circuits and low-pass filtered (the cut-off frequency f_c, which was in the range 400–1250 Hz depending on the transverse position of the probe, was set close to the Kolmogorov frequency $U_1/2\pi\eta$). The signals were then digitized into a personal computer using a 12 bit A/D converter at a sampling frequency, f_s, of 2500 Hz. The record duration was about 60 s. This was estimated to be long enough for the second- and third-order moments of Δu_1 and Δu_3 to converge.

4. Estimations of $\langle \epsilon \rangle$

Before considering the extended Kolmogorov equations, we first consider results for $\langle \epsilon \rangle$ obtained using different approaches. Four methods have been identified, each providing an estimate for comparison with the 'true' $\langle \epsilon \rangle$, given by (1.2). As already noted, an experimental estimation of this latter quantity is prohibitive. We have opted to identify $\langle \epsilon \rangle$ with the DNS estimates of it, as in Antonia, Zhou & Romano (1997*b*). The present experiment was performed for the same flow and Reynolds number as the numerical simulations (Kim, Moin & Moser 1987). Whilst one cannot expect exact similarity of conditions between the simulation and real flows, the simulation is able to estimate all the spatial derivatives with acceptable accuracy, provided the numerical resolution is adequate.

There have been several experimental attempts to approximate $\langle \epsilon \rangle$ in channel and pipe flows. Laufer (1954) measured up to five of the nine terms in the homogeneous form of $\langle \epsilon \rangle$ in a pipe flow; he used isotropy to infer the remaining terms. This method is laborious. Its accuracy depends, to a large extent, on the high-frequency response of the hot-wire equipment, the spatial resolution of the probes used and also the degree with which isotropy is satisfied. Departures from isotropy are accentuated as the wall is approached; the measurement inaccuracy of derivatives is further exacerbated as the magnitude of η decreases. In this flow region, the energy budget is likely to provide a better estimate of $\langle \epsilon \rangle$, notwithstanding the difficulty of measuring the diffusion term.

Many direct numerical simulations of the channel flow have been carried out since the original simulation of Kim *et al.* (1987). They all indicate (e.g. Mansour, Kim & Moin 1988; Kasagi & Shikazono 1995) that, in the wall region, the pressure diffusion is generally small by comparison to either $\partial_3 \langle u_3 u_i^2 \rangle$, the diffusion by the wall-normal velocity fluctuations, or the viscous diffusion.

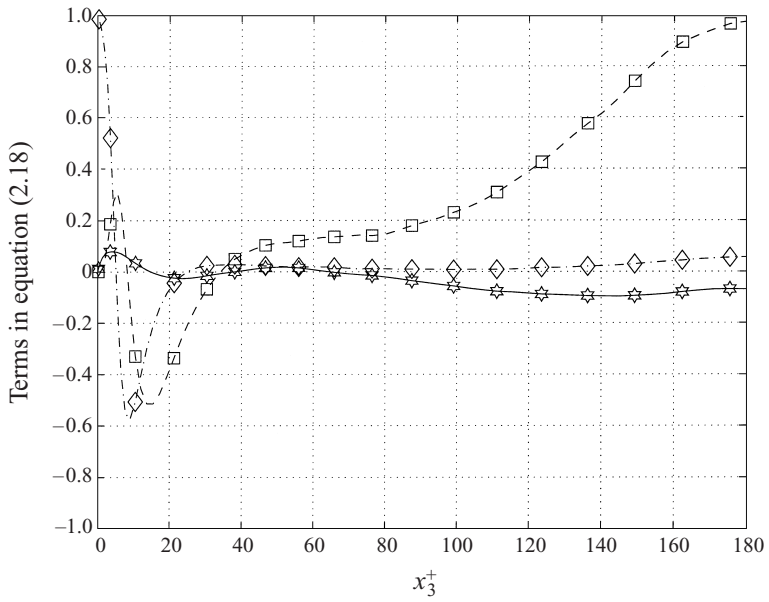

FIGURE 1. Normalized distributions of the three diffusion terms of (2.18). These terms have been normalized by $\langle\epsilon\rangle$. $x_3^+ \equiv x_3 U_\tau/\nu$, where U_τ is the friction velocity. The DNS data are from Kim *et al.* (1987): viscous diffusion ($\diamond$), turbulent diffusion ($\square$) and pressure diffusion ($*$).

The three diffusion terms in the energy budget equation, (2.18), are plotted, after normalization by $\langle\epsilon\rangle$, in figure 1. The DNS data are those of Kim *et al.* (1987). At the wall, viscous diffusion must balance $\langle\epsilon\rangle$ whereas at the centreline ($x_3^+ = 180$), the u_3-diffusion and $\langle\epsilon\rangle$ are approximately equal, in reasonable agreement with (2.19). The pressure-diffusion term, at the centreline, is less than 10% of the u_3-diffusion.

Lawn (1971) inferred $\langle\epsilon\rangle$ from the behaviour of the u_1-spectrum in the IR:

$$E(k_1) = K\langle\epsilon\rangle^{2/3} k_1^{-5/3},$$

with $K \approx 0.51$. The advantage of this approach is that the spectrum needs only to be accurately measured over a medium frequency range, as was noted by Bradshaw (1969). This is essentially the spectral equivalent of Kolmogorov's equation in the context of determining $\langle\epsilon\rangle$. Strictly, for compliance with Kolmogorov (1941), both approaches become more accurate as the Reynolds number increases, provided local isotropy is satisfied. Lawn also compared estimates of $\langle\epsilon\rangle$, obtained from different methods. He underlined that, even if the measurement of $\langle\epsilon\rangle$ is in error, the spectral method is robust and more likely to provide meaningful estimates when the Reynolds number is large enough. Although K has been shown to remain 'constant' down to $R_\lambda \simeq 100$ (e.g. Bradshaw 1969; Sreenivasan 1995), recent results (e.g. Antonia, Pearson & Zhou 2000) indicate that both the magnitude of the spectral exponent as well as that of K increase slowly with R_λ at least in the range $R_\lambda \lesssim 1000$; it is possible that constant values may be reached at much higher R_λ.

Eggels *et al.* (1994) used both direct numerical simulations and experiments to study a fully developed turbulent pipe flow. The agreement between the numerical and experimental results was good for lower-order statistics and reasonable for higher-order statistics. Various terms in the energy budget equation compared favourably using both approaches. However, the dissipation rate was inferred only from the

	Small scales	Large scales
Generalized Kolmogorov's equation (2.13)	$\widetilde{\langle\epsilon\rangle_{iso}} = 0.88$	$\widetilde{\langle\epsilon\rangle_{iso}^{LS}} = 1.32$
Generalized form of the extended Kolmogorov equation (2.23)	$\widetilde{\langle\epsilon\rangle_{hom}} = 0.85$	$\widetilde{\langle\epsilon\rangle_{hom}^{LS}} = 0.95$

TABLE 1. Ratios of various experimental estimations of $\langle\epsilon\rangle$ and the true (DNS) $\langle\epsilon\rangle$ on the channel flow centreline.

DNS data. Kim *et al.* (1987) also compared their turbulent channel flow simulation results with available existing experimental data at a comparable Reynolds number. Although the computed turbulence statistics were generally in good agreement with the experimental results, there were also discrepancies in the wall region, mainly due to the difficulty of adequately approximating $\langle\epsilon\rangle$ in the experiment.

In the light of the previous observations, it seems reasonable to use the numerical value of $\langle\epsilon\rangle$ as a reference against which estimates from the four methods identified in §§ 1 and 2 can be assessed. We recall here that (2.13) is consistent when $r \to 0$ with $\langle\epsilon\rangle \equiv \langle\epsilon\rangle_{iso}$, as given by (1.4), and, when $r \to \infty$, with $\langle\epsilon\rangle \equiv \langle\epsilon\rangle_{iso}^{LS}$, as given by (2.19). Also, (2.23) reduces to $\langle\epsilon\rangle \equiv \langle\epsilon\rangle_{hom}$, given by (1.3), when $r \to 0$, and to $\langle\epsilon\rangle \equiv \langle\epsilon\rangle_{hom}^{LS}$, given by (2.25). All four methods require measurements of different velocity components on the channel centreline. In order to estimate derivatives with respect to x_3 of different velocity components, we used simultaneous measurements of u_1 and u_3 at different x_3 positions. When estimating $\langle\epsilon\rangle_{iso}$ and $\langle\epsilon\rangle_{hom}$, only measurements on the axis were used, while for the other two estimates, off-axis measurements were also used. For example, in order to estimate $\langle\epsilon\rangle_{hom}^{LS}$ from $\partial_3\langle u_3 u_i^2\rangle$, values of $\langle u_3 u_i^2\rangle$ were obtained at different values of x_3, and the differentiation was carried out using finite differencing. The result does not depend on the range used for x_3, provided x_3 is sufficiently small.

Table 1 contains the four estimates of $\langle\epsilon\rangle$; the tilde denotes that these values have been normalized by the reference (DNS) value. A value of 1 represents perfect agreement with the 'true' $\langle\epsilon\rangle$. The value closest to 1 is obtained from the relation based on homogeneity and quasi-isotropy (two velocity components are used): $\langle\epsilon\rangle_{hom}^{LS}$ is within 5% of the DNS value. This result does not necessarily mean that a one-point approach will always be able to yield a reliable value for a quantity as complex as $\langle\epsilon\rangle$.

5. Validation of (2.13) and (2.23)

Here, we test the generalized forms of Kolmogorov's equations against measurement. Since these equations suppose local isotropy, we first consider isotropic relations such as (2.11) and (2.12). Figure 2(*a*) shows $NH_{33}(r)$, the terms on the left-hand side of (2.12), and term $\partial_3\langle u_3(\Delta u_3)^2\rangle(r)$, estimated from measurements and Taylor's hypothesis. A perfect validation of (2.12) requires these two sets of terms to be identical. For relatively large scales, the ratio of these terms is about 1.8. In figure 2(*b*), we represent the ratio $NH_{33}(r)/\partial_3\langle u_3(\Delta u_3)^2\rangle(r)$ (○) which is 1 for relatively small scales. We also represent the ratio $D_{33}(r)/\langle(\Delta u_3)^2\rangle$ (□) which is close to the value 1 for small scales, and different from 1 for larger scales. A value 1 for this latter ratio validates (2.11). The conclusion we draw from this figure is that (2.12) is verified by experimental data to (approximately) the same degree as relation (2.11) is experimentally satisfied. It is not surprising that such (quasi)-isotropic relations are not well-satisfied for large

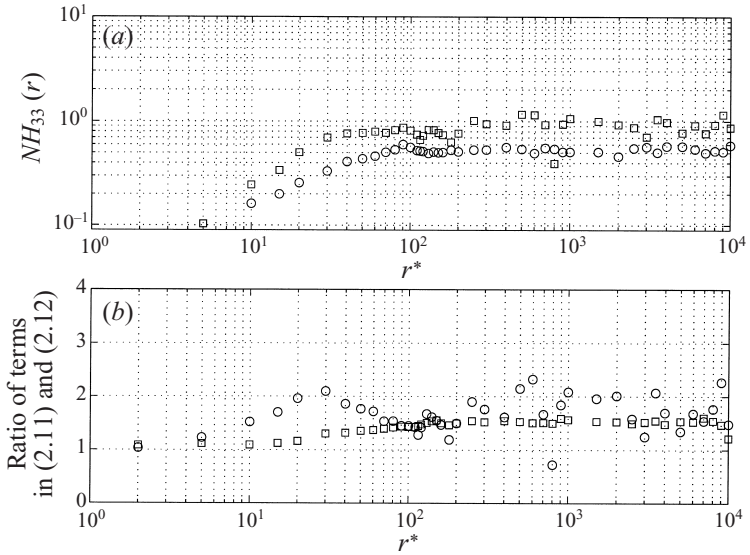

FIGURE 2. Isotropy tests associated with the quantities $NH_{33}(r)$ and $D_{33}(r)$. (*a*) ○, Measured $NH_{33}(r)$; □, $NH_{33}(r)$ inferred from $NH_{11}(r)$ using relation (2.12). (*b*) ○, Ratios of the $NH_{33}(r)$ values inferred using relation (2.12) and those measured; □, ratios for $D_{33}(r)$ obtained using relation (2.11) and those measured.

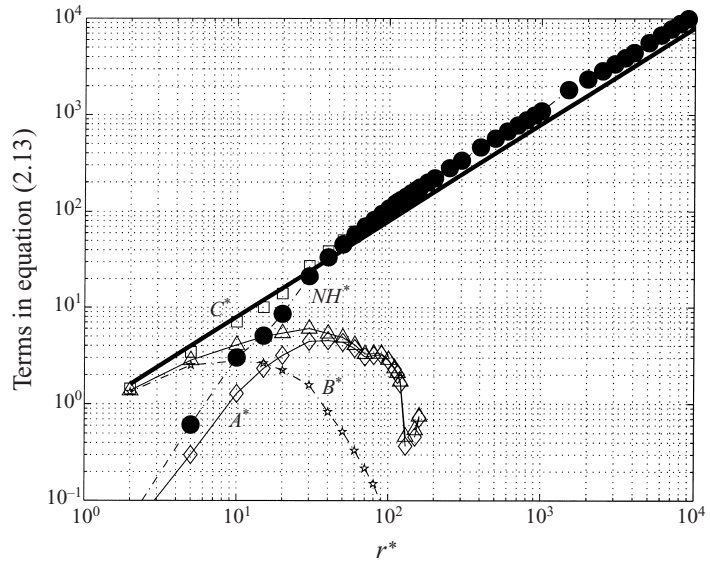

FIGURE 3. Verification of (2.13): turbulent transport term A^* (–◇–), small-scale diffusion term B^* (–∗–∗–), A^*+B^* (–△–), non-homogeneous term NH^* (–●–●–). $A^*+B^*+NH^*$ (□) is to be compared with C^* (bold solid line).

scales, even on the channel axis. But an important step forward can be made by (only) considering the extra non-homogeneous term $NH(r)$ in (2.13) and (2.23).

The terms in the non-dimensional form of (2.13) are shown in figure 3 (a superscript $*$ denotes normalization by Kolmogorov scales). Note that at this small Reynolds number, there is no IR; we can however identify a restricted scaling range (RSR)

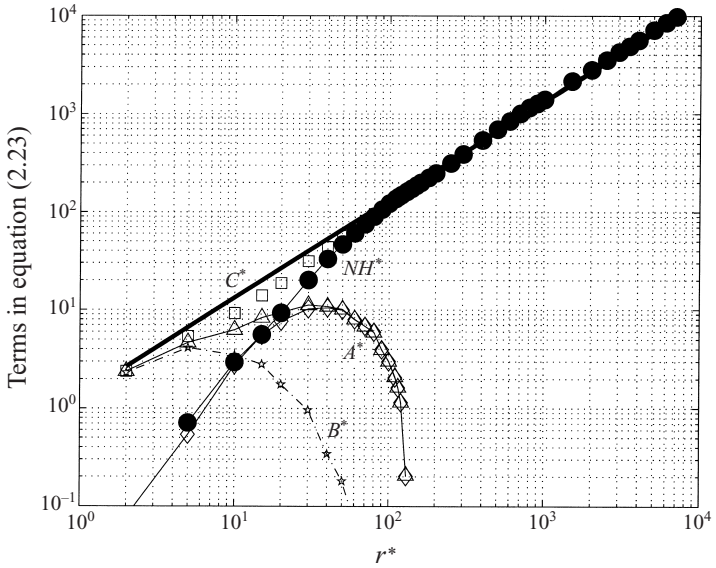

FIGURE 4. Verification of (2.23): turbulent transport term A^* (–◇–), small-scale diffusion term B^* (–∗–∗–), $A+B$ (–△–), non-homogeneous term NH^* (–●–). $A^*+B^*+NH^*$ (□) is to be compared with C^* (bold solid line).

given by $15 < r^* < 40$ (e.g. Antonia, Orlandi & Romano 1998) in which A is quasi-linear. The supplementary term NH has been obtained in similar fashion to $\langle\epsilon\rangle_{iso}^{LS}$, i.e. $\langle u_3(\Delta u_1)^2\rangle$ was estimated on the axis, and at different positions away from the axis. The x_3-derivative of these moments is then estimated by finite differencing and NH was evaluated by integrating from $r = 0$, corresponding to $NH \equiv 0$. $NH(r)$ is small for small scales, and increases as the scale increases. Equation (2.13) is satisfied to an accuracy of about 10% for the very small and intermediate scales. The sum $A^*+B^*+NH^*$ is 10% smaller than C^* ($\equiv 4r^*/5$). This behaviour is consistent with our previous result: the limit for the very small scales of the terms in (2.13) is consistent with the isotropic definition of $\langle\epsilon\rangle_{iso}$, or (see table 1) $\langle\epsilon\rangle_{iso}$ is 12% smaller than $\langle\epsilon\rangle$. On the other hand, for the very large scales, (2.13) corresponds to $\langle\epsilon\rangle_{iso}^{LS}$ which over-estimates $\langle\epsilon\rangle$ by 35%. This result re-emerges in figure 3, where the sum $A^*+B^*+NH^*$ is about 40% larger than C^* for the very large scales. In the RSR, NH is even more important than A, reflecting the dominance of large-scale phenomena at this relatively small Reynolds number. It is also worth emphasizing that the use of $\langle\epsilon\rangle_{iso}$, instead of $\langle\epsilon\rangle$, satisfies (2.13) perfectly for the dissipative scales whereas, for the large scales, the disagreement is as large as 50%. This value is obviously given by the ratio $\langle\epsilon\rangle_{iso}^{LS}/\langle\epsilon\rangle_{iso}$. Such a verification for the small scales has previously been found (Antonia *et al.* 1997*b*) in relation to the classical Kolmogorov equation. Similarly, when using $\langle\epsilon\rangle_{iso}^{LS}$ instead of the real $\langle\epsilon\rangle$, perfect verification is obtained for very large scales, while the disagreement is very important for the dissipative scales.

All terms in (2.23) are displayed in figure 4. Here, mixed moments such as $\langle u_3(\Delta u_1)^2\rangle$ and $\langle u_3(\Delta u_3)^2\rangle$ have been calculated in order to obtain the new supplementary term. The magnitude of the additional term (NH) decreases as the scale decreases. For very small scales, (2.23) is verified with an accuracy of 10%, in agreement with the ability of $\langle\epsilon\rangle_{hom}$ to approximate $\langle\epsilon\rangle$. For very large scales, the accuracy is about 5%, also in accord with the differences between $\langle\epsilon\rangle_{hom}^{LS}$ and $\langle\epsilon\rangle$. Note the significant improvement

of the generalized budget equation, relative to (2.13), especially for the very large scales. To highlight the degree to which the new equations are satisfied, the ratio

$$\mathscr{R} \equiv \frac{(A^* + B^* + NH^*)}{C^*}, \tag{5.1}$$

which corresponds to (2.23), is shown in figure 6, below. Ideally, $\mathscr{R}$ should be equal to 1. The actual value is 0.9 for the very small scales, and 0.95 for the very large scales. For the latter scales, the equation is very well satisfied, implying that the main phenomenon responsible for the equilibrium state of the flow is indeed the large-scale non-homogeneity.

Equation (2.23) is better verified than (2.13) especially for very large scales, indicating that all velocity components play a different role in the energy budget. For intermediate scales ($5\eta \leqslant r \leqslant 40\eta$), (2.23) is verified to an accuracy of only 30%, since $\mathscr{R} \simeq 0.7$ in the RSR. For each set of data, $\mathscr{R}$ displays a marked concave curvature with the minimum (dip) occurring near the centre of the RSR. This may be due to poor measurement accuracy, inadequate estimation of derivatives, and the fact that the overall budget contains terms which reflect different phenomena: A (turbulent advection), B (molecular diffusion) and NH (sign of the small non-homogeneity associated with large scales). The dip appears in the 'transition' between very large and very small scales. Note however the improvement vis-à-vis the classical Kolmogorov equation, for which $A^*/C^* \approx 0.3$.

The discrepancy for intermediate and small scales, even at the centre of the channel, is presumably due to the lack of isotropy and homogeneity. This remark leads us to the conclusion that the hypotheses used in deriving (2.13) and (2.23) are very intricate concepts. There is therefore a need to revise them as well as the mathematical manipulations required in order to best capture the important physics of the flow. The emerging message is that the channel flow is more complex than grid turbulence for which quite good results were obtained (see Danaila *et al.* 1999). Grid turbulence is characterized by good local homogeneity and isotropy, and by a large-scale non-homogeneity or non-stationarity. A more extended and realistic characterization is obviously needed for the channel flow.

6. A generalized form of the extended Kolmogorov equation following relaxation of local homogeneity

We return here to the derivation of (2.23) to gain more insight into its imperfect validation in the RSR. Since we characterize this flow by a large-scale non-homogeneity as well as local homogeneity and isotropy, it is possible that, at this small Reynolds number, even the RSR scales could be contaminated by a weak local non-homogeneity. Thus, starting from (2.4), special attention is given to the second term $\Delta(u_\alpha)\partial^+_\alpha(\Delta u_i)$, which transforms to $\Delta(u_\alpha)[\partial(\Delta u_i)/\partial r_\alpha]$, using definitions (2.5). Our approach is then to revisit definitions (2.5), especially in what concerns the derivative at $\boldsymbol{x}^+$, separated by $\boldsymbol{r}$ from point $\boldsymbol{x}$. As emphasized by Hill (1997) and in our discussion following (2.10), the derivative with respect to $\boldsymbol{X} = (\boldsymbol{x} + \boldsymbol{x}^+)/2$ is negligible when local homogeneity prevails. The possibility of a small local non-homogeneity cannot be discounted even at the centre of the channel and the inclusion of the derivative with respect to $\boldsymbol{X}$ seems unavoidable. Thus,

$$\partial^+_\alpha \equiv \left(\frac{\partial}{\partial r_\alpha}\right) + \frac{1}{2}\frac{\partial}{\partial X_\alpha}, \quad \partial_\alpha \equiv -\left(\frac{\partial}{\partial r_\alpha}\right) + \frac{1}{2}\frac{\partial}{\partial X_\alpha}, \tag{6.1}$$

so that $\partial/\partial X_\alpha = \partial_\alpha + \partial_\alpha^+$. The new derivative just reflects a small local non-homogeneity for intermediate scales. This is considered to be a relaxed form of local homogeneity, since, whilst homogeneity and isotropy are assumed for some of the terms in (2.4), new terms involving the derivative with respect to $\boldsymbol{X}$ are considered. In a physical sense, the small local non-homogeneity is the extended effect of the larger scales on the smaller scales. Thus,

$$\Delta(u_\alpha)\partial_\alpha^+(\Delta u_i) = \Delta(u_\alpha)\frac{\partial(\Delta u_i)}{\partial r_\alpha} + \frac{1}{2}\Delta(u_\alpha)\frac{\partial}{\partial X_\alpha}(\Delta u_i). \tag{6.2}$$

By taking into account the new term, proceeding in similar fashion to the derivation of (2.23), by multiplying with $2\Delta u_i$ and averaging, we obtain

$$\begin{aligned}(\partial_t + U_1\partial_1)\langle(\Delta u_i)^2\rangle(\boldsymbol{r}) + \left(\frac{\partial}{\partial r_\alpha} + \frac{1}{2}\frac{\partial}{\partial X_\alpha}\right)\langle\Delta(u_\alpha)(\Delta u_i)^2\rangle(\boldsymbol{r}) \\ +[\partial_\alpha^+ + \partial_\alpha]\langle u_\alpha(\Delta u_i)^2\rangle(\boldsymbol{r}) \\ = -2(\partial_i + \partial_i^+)\langle\Delta p\Delta u_i\rangle(\boldsymbol{r}) + 2\nu\langle\Delta u_i(\partial_\alpha^2 + \partial_\alpha^{2+})(\Delta u_i)\rangle(\boldsymbol{r}).\end{aligned} \tag{6.3}$$

Note here that the same kind of approach (e.g. relations (6.1)) could be used in order to investigate the effect of the local non-homogeneity in the dissipative range, by applying the same rule for term B, which contains the second derivative with respect to $\boldsymbol{x}^+$. This calculation leads finally to the need for estimating the second derivative with respect to X_α, and thus to x_3 in our case, using experimental data.

Using local isotropy for those terms characterizing RSR phenomena, and approximate local isotropy for the supplementary terms such as the non-homogeneous term NH, any dependence on $\boldsymbol{r}$ becomes a dependence on r only, and could be measured along the stream direction. Neglecting the pressure term, (6.3) reduces to

$$\begin{aligned}(\partial_t + U_1\partial_1)\langle(\Delta u_i)^2\rangle + \left(\frac{\partial}{\partial r_\alpha} + \frac{1}{2}\frac{\partial}{\partial X_\alpha}\right)\langle\Delta(u_\alpha)(\Delta u_i)^2\rangle \\ +[\partial_\alpha^+ + \partial_\alpha]\langle u_\alpha(\Delta u_i)^2\rangle(\boldsymbol{r}) = 2\nu\left[\frac{\partial^2}{\partial {r_\alpha}^2} + \frac{1}{4}\frac{\partial^2}{\partial {X_\alpha}^2}\right]\langle(\Delta u_i)^2\rangle - 4\langle\epsilon\rangle,\end{aligned} \tag{6.4}$$

which is generally valid for all scales in any nearly locally isotropic flows or flow regions such as

grid turbulence, where $U_1\partial_1\langle\ \rangle$ is the only extra term relative to the classical Kolmogorov terms equation;

centreline of a channel flow, where the extra term is $\partial_3\langle\ \rangle$;

centreline of a jet flow, where both $U_1\partial_1\langle\ \rangle$ and the lateral turbulent diffusion term need to be retained.

In this work, we only consider the effect of the non-homogeneity on the 'inertial' term A, via relation (6.2), and we simply neglect the term $\partial^2/\partial {X_\alpha}^2\langle(\Delta u_i)^2\rangle$ in (6.4). This is worth pursuing in future.

Finally, on the centreline of a channel flow, using the stationarity of this flow in a fixed reference frame, the x_1 homogeneity, the fact that $(1/2)\partial/\partial X_\alpha\langle\ \rangle = (1/2)(\partial_\alpha + \partial_\alpha^+)\langle\ \rangle \equiv \partial_3\langle\ \rangle$ and assuming that $\partial_3\langle\Delta u_3(\Delta u_i)^2\rangle$ depends on r only, we obtain

$$-\langle\Delta u_1(\Delta u_i)^2\rangle + 2\nu\frac{\mathrm{d}}{\mathrm{d}r}\langle(\Delta u_i)^2\rangle + \frac{1}{r^2}\int_0^r y^2[-2\partial_3\langle u_3(\Delta u_i)^2\rangle - \partial_3\langle\Delta u_3(\Delta u_i)^2\rangle]\mathrm{d}y = \tfrac{4}{3}\langle\epsilon\rangle r \tag{6.5}$$

or, in dimensionless form,

$$A^* + B^* + NH^* + LNH^* = C^*,$$

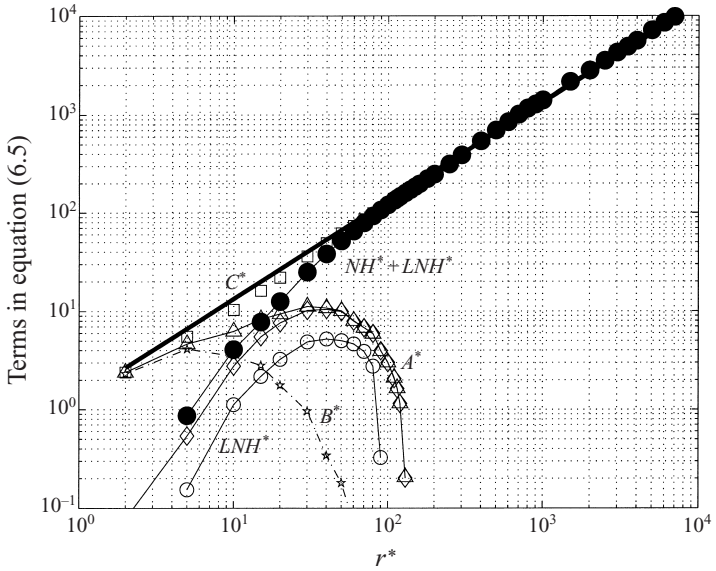

FIGURE 5. Verification of (6.5), which includes a term relaxing local homogeneity, LNH^*(–○–): turbulent transport term A^* (–◇–), small-scale diffusion term B^* (–∗–∗–), $A+B$ (–△–), NH^*+LNH^* (–●–). $A^*+B^*+NH^*+LNH^*$ (□) is to be compared with C^* (bold solid line).

where the new term *LNH* expresses the local non-homogeneity. Note that *NH* and *LNH* could also be written as

$$NH + LNH = -\frac{1}{r^2}\int_0^r y^2 \partial_3 \langle (u_3 + u_3^+)(\Delta u_i)^2 \rangle \mathrm{d}y.$$

Figure 5 displays all the terms in (6.5). While A^*, B^* and C^* are obviously the same as in (2.23) (illustrated in figure 4), the new term LNH^* improves the balance over the RSR. *LNH* has been computed in similar manner to all the other new terms which contain an x_3-derivative. This derivative acts on moments such as $\langle \Delta u_3 (\Delta u_1)^2 \rangle$ and $\langle (\Delta u_3)^3 \rangle$, which are zero for very small and very large scales. Thus, the validation of (2.23) is unaltered for very small and very large scales. The inclusion of the small local non-homogeneity appears as a supplementary term which is important only in the RSR. The accuracy with which the new equation is satisfied is about 10% in the range $r \gtrsim 20\eta$.

Figure 6 shows the ratios of different terms in (6.5). Except for the new term *LNH*, all the others are the same as in (2.23). The ratio $(A^*+B^*+NH^*+LNH^*)/C^*$ is now within 10% of the theoretical value of 1. For smaller scales, isotropy and local homogeneity should be used more cautiously. Equation (6.5) can be seen as a practical means of determining $\langle \epsilon \rangle$. Let us now suppose that another channel flow is being investigated, one for which DNS estimates of $\langle \epsilon \rangle$ are not available. By measuring u_1 and u_3 at different x_3 positions around the centreline, one can estimate A, B, NH and LNH in (6.5). A compensated representation of the sum of these terms, divided by $(4/3)r$, should yield a plateau which extends from intermediate to large scales, and presumably provide a more reliable estimate of $\langle \epsilon \rangle$. In such a compensated representation, all the significant phenomena contributing to the equilibrium of the flow emerge: the small non-homogeneity of the large scales (*NH*), the local non-homogeneity and advection (*LNH* and *A*) at intermediate scales and the dissipative effects for the very small scales.

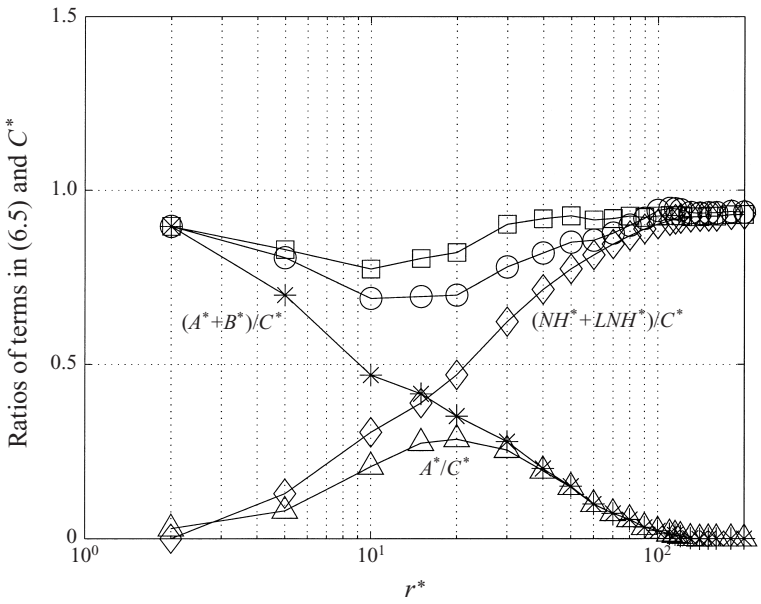

FIGURE 6. Ratios of terms in (6.5) and C^*: A^*/C^* (–△–), $(A^*+B^*)/C^*$ (–∗–∗–), $(NH^*+LNH^*)/C^*$ (–◇–), $\mathscr{R} \equiv (A^*+B^*+NH^*)/C^*$ (–○–) and $(A^*+B^*+NH^*+LNH^*)/C^*$ (–□–).

Thus, an important practical implication of (6.6) is that a proper estimate of $\langle\epsilon\rangle$ is possible on the centreline of a channel flow, for moderate Reynolds numbers, to an accuracy of 10%, by measuring two velocity fluctuations and taking account of the large-scale non-homogeneity as well as including a relaxed form of local homogeneity.

A large-scale balance is not possible for such an equation when the flow is anisotropic. In this case, the gradient and Laplacian operators involved in (6.4) cannot assume a simple isotropic form, and, more importantly, relations (2.11) and (2.12), which reflect the quasi-isotropic properties of $NH_{ij}(\boldsymbol{r})$, will no longer be valid. In this respect, we have analysed (6.5) away from the channel axis, at $x_3/h = 0.4$, in similar manner to that already described for the centreline region, i.e. using the 'true' $\langle\epsilon\rangle$ from DNS data. While the equation is not balanced for the small scales ($\langle\epsilon\rangle_{iso}/\langle\epsilon\rangle \approx 0.45$), the error is approximately the same as the scale increases. For this particular location, $\lim_{r\to\infty}(A^*+B^*+NH^*+LNH^*)/C^* \approx 0.5$, simply because, according to the large-scale limits previously presented, $\langle\epsilon\rangle_{hom}/\langle\epsilon\rangle \approx 0.5$. This result reflects the complexity of sheared flows, for which the true $\langle\epsilon\rangle$ cannot be estimated satisfactorily through simple hypotheses.

Another important implication of this study concerns small-scale intermittency. We have emphasized the role played by the small (large-scale) non-homogeneity when determining the correct energy budget equation at each scale, implicitly implying that the scaling range determined solely from $\langle(\Delta u_1)^3\rangle$ is probably irrelevant. Thus, high-order scaling exponents should be determined with caution in slightly non-homogeneous flows at small to moderate Reynolds numbers.

7. Conclusions

Generalized forms of the Kolmogorov equation have been proposed and verified on the centreline of a fully developed turbulent channel flow. The new equations

take into account the small non-homogeneity of the large scales, which acts along the direction normal to the wall. An interesting aspect of the equations is that they essentially represent budget equations for the energy at different scales.

Equation (2.13), which is the generalized form of the classical Kolmogorov equation, is an improvement with respect to the classical four-fifths law. However, there is a disagreement of about 50% between very small and very large scales, apparently due to the anisotropy of the flow. This provided the motivation for deriving another extended version of Kolmogorov's equation, which includes all the velocity components. This equation is the analogue of Yaglom's four-thirds law (Antonia *et al.* 1997*a*). Taking account of the large-scale non-homogeneity results in a significant improvement of the budget, the disagreement being typically about 10% for very small scales and 5% for very large scales. There remains however a 30% departure over a restricted scaling range. Local homogeneity was subsequently relaxed by including a small local non-homogeneity. This represents an extension into the restricted scaling range of the local non-homogeneity which acts at very large scales. Mathematically, this hypothesis is equivalent to considering derivatives of the third-order moments with respect to x_3, the non-homogeneous direction. The new equation (6.5) is satisfied to within 10% for intermediate and very large scales. This equation is the main result of the paper. An important application of this equation is that it provides a means of experimentally determining the mean energy dissipation rate on the centreline of a fully developed turbulent channel flow.

R. A. A. acknowledges the support of the Australian Research Council. L. D. is most grateful to Professor M. Coantic for useful discussions.

Appendix A. Justification of relations (2.11) and (2.12)

Here, the tensor $NH_{ij}(\boldsymbol{r})$, given by relation (2.10), is shown to exhibit similar mathematical properties to those of an isotropic second-order tensor. Generally, these kinds of tensors feature in second-order structure functions. For simplicity and to follow as closely as possible the analysis in MY, we consider the correlation tensors which correspond to these structure functions. We define

$$BNH_{ij}(\boldsymbol{r}) \equiv \partial_3 \langle u_3 u_i u_j^+ \rangle (\boldsymbol{r}), \tag{A 1}$$

which is similar to definition (12.26) in MY for the correlation tensor $B_{ij}(\boldsymbol{r})$. Starting from the premise that $B_{ij}(\boldsymbol{r})$ is isotropic, we shall further demonstrate that $BNH_{ij}(\boldsymbol{r})$ also presents some quasi-isotropic properties. The same tensorial analysis (developed in an isotropic context) as in MY (pp. 38, 39) will be adapted to our non-homogeneous tensor $BNH_{ij}(\boldsymbol{r})$. We first project these tensors onto a special set of coordinates (x_1', x_2', x_3'), the axis x_1' being along the vector $\boldsymbol{r}$. The magnitudes of the components of the tensors $B_{ij}(\boldsymbol{r})$ and $BNH_{ij}(\boldsymbol{r})$ in this new coordinate system will be denoted by $B_{ij}'(r)$ and $BNH_{ij}'(r)$; note the dependence is on r only.

The tensor $BNH_{ij}'(r)$ can be expressed (Appendix B) in the form

$$BNH_{ij}'(r) \equiv \mathscr{L}\left(\frac{\partial}{\partial x_k'} \langle u_k' u_i' u_j'^+ \rangle\right)(r), \tag{A 2}$$

to relatively good accuracy, with summation applying when k is repeated. $\mathscr{L}$ is a linear combination of terms with the form specified within the brackets. According to (A 2), the form of the second-order tensor, $BNH_{ij}'(\boldsymbol{r})$, involves, in the new reference system, only terms containing velocity components u_k', and derivatives with respect to x_k'. This

is important for the next step in our approach. It can now be readily appreciated that any change associated with x'_k will affect the sign of $BNH'_{ij}(r)$ only via x'_i and x'_j, as for the classical isotropic tensor $B'_{ij}(r)$ (cf. MY). A rotation of π about the axis x'_1 results in the reversal of the directions x'_2 and x'_3, so that $B'_{12}(r) = -B'_{12}(r) = 0$. For the same transformation, we now examine the tensor $BNH'_{12}(r)$, written using the form (A 2). For every $k = 1, 2, 3$, due to the fact that the orientation of the axis x'_k appears twice (first, because of the derivative, secondly, because of the velocity component u_k), $BNH'_{12}(r)$ will exhibit the same symmetry as $B'_{12}(r)$. It follows that

$$BNH'_{12}(r) = -BNH'_{12}(r) = 0.$$

Similarly, it can be shown that

$$BNH'_{13}(r) = BNH'_{21}(r) = BNH'_{31}(r) = 0. \tag{A 3}$$

Rotation about any axis leads to interchanging the other two axes, whereas reflection in a plane, for example (x'_1, x'_2), results in replacing x'_3 by $-x'_3$. Despite this change in sign, the term $\partial_{x'_3}\langle u'_3 u'_i u'_j\rangle(r)$ will retain the same properties as $\langle u'_i u'_j\rangle(r)$, i.e.

$$BNH'_{23}(r) = BNH'_{32}(r) = 0, \quad BNH'_{22}(r) = BNH'_{33}(r). \tag{A 4}$$

As a first conclusion, all the symmetry properties of the tensor $BNH'_{ij}(r)$ are identical to those of the isotropic tensor $B'_{ij}(r)$. Consequently, the tensors $B_{ij}(\boldsymbol{r})$ and $BNH_{ij}(\boldsymbol{r})$ will also have similar properties and may be written using only two non-equal components (longitudinal and normal) as in relation (12.27) of MY. For the tensor $BNH_{ij}(\boldsymbol{r})$, these two distinct components are

$$\left.\begin{aligned} BNH'_{11}(r) = BNH_{LL}(r) = \partial_3\langle u_3 u'_1 u'^{+}_1\rangle(r), \\ BNH'_{33}(r) = BNH_{NN}(r) = \partial_3\langle u_3 u'_3 u'^{+}_3\rangle(r). \end{aligned}\right\} \tag{A 5}$$

Note that, the derivative ∂_3 and the velocity component u_3 in the above relations are, for simplicity, kept in the basic reference system, instead of using $\partial/\partial x'_k$ and u'_k.

The second-order tensor $BNH_{ij}(\boldsymbol{r})$ is written using (A 5) as

$$BNH_{ij}(\boldsymbol{r}) = \left[BNH'_{11}(r) - BNH'_{33}(r)\right]\frac{r_i r_j}{r^2} + BNH'_{33}(r)\delta_{ij}, \tag{A 6}$$

while incompressibility leads to

$$BNH'_{33}(r) = BNH'_{11}(r) + \frac{r}{2}\frac{\mathrm{d}}{\mathrm{d}r}BNH'_{11}(r), \tag{A 7}$$

which is similar to relation (12.67) of MY. The function $BNH_{ij}(\boldsymbol{r})$ has therefore similar properties to $B_{ij}(\boldsymbol{r})$.

For the above reasons, structure functions $D_{ij}(\boldsymbol{r})$ and $NH_{ij}(\boldsymbol{r})$ have similar properties, i.e. they can be expressed in terms of the longitudinal structure functions (depending only on separations along any spatial direction, e.g. x_1) via similar relations, e.g.

$$D_{33}(r) = D_{11}(r) + \frac{r}{2}\frac{\mathrm{d}}{\mathrm{d}r}D_{11}(r), \tag{A 8}$$

and

$$NH_{33}(r) = NH_{11}(r) + \frac{r}{2}\frac{\mathrm{d}}{\mathrm{d}r}NH_{11}(r). \tag{A 9}$$

Appendix B. Justification of relation (A 2)

By taking into account the slight non-homogeneity along x_3, and the homogeneity (equation (2.9)) along both x_1 and x_2, we can examine the properties of the flow, about the non-homogeneous (x_3) direction. The planes (x_1, x_3) and (x_2, x_3) are from this point of view equivalent, since any rotation about the x_3-axis should lead to a new reference system (x_1', x_2', x_3), with properties

$$\partial_1'\langle\ \rangle = \partial_2'\langle\ \rangle \equiv 0, \quad \partial_3\langle\ \rangle \neq 0,$$

identical to those of the reference system (x_1, x_2, x_3), cf. relations (2.9).

It is therefore sufficient to consider what happens when the separation vector $\boldsymbol{r}$ is in the (x_1, x_3)-plane. Suppose the angle between $\boldsymbol{r}$ and the axis x_1 is $\theta \in [0, \pi/2]$. Because of symmetry, these limits are sufficient. We then rotate the axes x_1 and x_3 through an angle θ so as to obtain the new reference system (x_1', x_3'), with one axis along $\boldsymbol{r}$. We have

$$x_1' = x_1 \cos\theta + x_3 \sin\theta, \quad x_3' = -x_1 \sin\theta + x_3 \cos\theta. \tag{B 1}$$

Inversely,

$$x_1 = x_1' \cos\theta - x_3' \sin\theta, \quad x_3 = x_1' \sin\theta + x_3' \cos\theta. \tag{B 2}$$

The tensor $BNH_{ij(\boldsymbol{r})}$ may be expressed, see (A 1), as a function of terms like $\langle(\partial_3 u_3)u_i u_j^+\rangle$, $\langle u_3(\partial_3 u_i)u_j^+\rangle$, etc. We now turn our attention to the first term, since all the others can be treated in a similar manner. By switching to the new reference system, we have

$$\begin{aligned}\partial_3 u_3 &= \left[\frac{\partial}{\partial x_1'}\sin\theta + \frac{\partial}{\partial x_3'}\cos\theta\right][u_1'\sin\theta + u_3'\cos\theta] \\ &= \frac{\partial u_1'}{\partial x_1'}\sin^2\theta + \left[\frac{\partial u_3'}{\partial x_1'} + \frac{\partial u_1'}{\partial x_3'}\right]\cos\theta\sin\theta + \frac{\partial u_3'}{\partial x_3'}\cos^2\theta.\end{aligned} \tag{B 3}$$

The first and third terms on the second line of (B 3) lead, after multiplying with any combination $u_i u_j^+$, to terms possessing the form indicated in (A 2). We now enquire into the 'cross' term, i.e. the second term on the second line of (B 3). The aim is to show that this term is zero, to relatively good accuracy. This term contains a product $\cos\theta\sin\theta$, so it is maximum when $\theta = \pi/4$. After rotating the original reference system through $\pi/4$, $\cos\theta = \sin\theta = \sqrt{2}/2$, we consider any combination between a 'cross' term $(\partial u_1'/\partial x_3')$ and any other pair of velocity components, e.g. $\langle(\partial u_1'/\partial x_3')u_1' u_3'^+\rangle$, in the basic reference system. Since relations (2.9) apply only for this system, we have, after using (B 1) and (B 2),

$$\begin{aligned}\left\langle \frac{\partial u_1'}{\partial x_3'}u_1' u_3'^+ \right\rangle &= \tfrac{1}{4}\left\langle[-\partial_1 + \partial_3](u_1 + u_3)(u_1 + u_3)\left[-u_1^+ + u_3^+\right]\right\rangle \\ &= \tfrac{1}{4}\left\langle[-\partial_1 u_1 - \partial_1 u_3 + \partial_3 u_1 + \partial_3 u_3](u_1 + u_3)(-u_1^+ + u_3^+)\right\rangle.\end{aligned} \tag{B 4}$$

After rearranging the terms, recalling that u_i^+ depends only on $\boldsymbol{x}^+$, and not on $\boldsymbol{x}$, and using relations (2.9), we obtain

$$\left\langle \frac{\partial u_1'}{\partial x_3'}u_1' u_3'^+ \right\rangle = \tfrac{1}{8}\partial_3\langle(u_1 + u_3)^2(u_3^+ - u_1^+)\rangle = 0, \tag{B 5}$$

since $\langle(u_1 + u_3)^2(u_3^+ - u_1^+)\rangle$ is zero by homogeneity and local isotropy. This result

was verified experimentally, and we have obtained that, for the smallest scale, $\langle (u_1 + u_3)^2(u_3^+ - u_1^+)\rangle(3\eta) = 0.3\langle (u_1 + u_3)^2 u_1^+\rangle(3\eta)$, while, for all other scales, these two-point correlations are zero.

Similarly, it can be shown (we do not reproduct the calculations here, but the approach is as outlined above) that

$$\left\langle \frac{\partial u_3'}{\partial x_1'} u_3' u_1'^+ \right\rangle = \tfrac{1}{8}\partial_3\langle (u_1 - u_3)^2(u_1^+ + u_3^+)\rangle \equiv 0. \tag{B 6}$$

Other combinations are negligible, since, by local isotropy and relations (2.9)

$$\left\langle \frac{\partial u_3'}{\partial x_1'} u_1' u_3'^+ \right\rangle = \left\langle \frac{\partial u_3'}{\partial x_1'} u_3' u_1'^+ \right\rangle = 0.$$

The first equality was verified experimentally, and the second corresponds to relation (B 6). Further,

$$\left\langle \frac{\partial u_1'}{\partial x_3'} u_3' u_1^{+\prime} \right\rangle \approx \left\langle \frac{\partial u_1'}{\partial x_3'} u_1' u_3^{+\prime} \right\rangle = 0,$$

where the first part of this approximation is verified by experiment, and the second corresponds to relation (B 5). All other combinations, containing an odd number of the same axis index, are zero by local isotropy. For example, $\langle (\partial u_3'/\partial x_1')u_1' u_1^{+\prime}\rangle = 0$, since, by changing x_3' to $-x_3'$, and keeping x_1' unchanged (i.e. by rotating through π in a plane perpendicular to x_1'), this term changes sign once, so it is zero by local isotropy. Further, any cross-combination involving one u_2' component will also be zero. For example, $\langle (\partial u_3'/\partial x_1')u_1' u_2^{+\prime}\rangle$ is zero, since a rotation of π about x_3' transforms x_1' to $-x_1'$ and x_2' to $-x_2'$, so that the term changes sign once and must be zero by local isotropy. Relation (A 2) therefore applies on the channel centreline.

REFERENCES

Anselmet, F., Gagne, Y., Hopfinger, E. J. & Antonia, R. A. 1984 High-order velocity structure functions in turbulent shear flows. *J. Fluid Mech.* **140**, 163.

Antonia, R. A., Chambers, A. J. & Browne, L. W. B. 1983 Relations between structure functions of velocity and temperature in a turbulent jet. *Exps. Fluids* **1**, 213.

Antonia, R. A., Kim, J. & Browne, L. W. B. 1991 Some characteristics of small-scale turbulence in a turbulent duct flow. *J. Fluid Mech.* **233**, 369.

Antonia, R. A., Orlandi, P. & Romano, G. P. 1998 Scaling of longitudinal velocity increments in a fully developed turbulent channel flow. *Phys. Fluids* **10**, 3239.

Antonia, R. A., Ould-Rouis, M., Anselmet, F. & Zhu, Y. 1997*a* Analogy between predictions of Kolmogorov and Yaglom. *J. Fluid Mech.* **332**, 395.

Antonia, R. A., Pearson, B. R. & Zhou, T. 2000 Reynolds number dependence of second-order velocity structure functions. *Phys. Fluids* **12**, 3000.

Antonia, R. A., Zhou, T. & Romano, G. P. 1997*b* Second- and third- order longitudinal velocity structure functions in a fully developed turbulent channel flow. *Phys. Fluids* **9**, 3465.

Bradshaw, P. 1969 Conditions for the existence of an inertial subrange in turbulent flow. *Aero. Res. Counc. R. & M.* 3603.

Danaila, L., Anselmet, F., Zhou, T. & Antonia, R. A. 1999 A generalization of Yaglom's equation which accounts for the large-scale forcing in heated decaying turbulence. *J. Fluid Mech.* **391**, 359.

Eggels, J. G. M., Unger, F., Weiss, M. H., Westerweel, J., Adrian, R. J., Friedrich, R. & Nieuwstadt, F. T. M. 1994 Fully developed turbulent pipe flow: a comparison between direct numerical simulation and experiment. *J. Fluid Mech.* **268**, 175.

Frisch, U. 1995 *Turbulence: The Legacy of A. N. Kolmogorov*. Cambridge University Press.

HILL, R. J. 1997 Applicability of Kolmogorov's and Monin's equations of turbulence. *J. Fluid Mech.* **353**, 67.

KASAGI, N. & SHIKAZONO, N. 1995 Contribution of direct numerical simulation to understanding and modelling turbulent transport. *Proc. R. Soc. Lond.* A **451** 257.

KIM, J., MOIN, P. & MOSER, R. 1987 Turbulence statistics in fully developed channel flow at low Reynolds numbers. *J. Fluid Mech.* **177**, 133.

KOLMOGOROV, A. N. 1949 The local structure of turbulence in incompressible viscous fluid for very large Reynolds numbers. *Dokl. Akad. Nauk. SSSR* **30** 299. [English translation in 'Turbulence and stochastic processes: Kolmogorov's ideas 50 years on', *Proc. R. Soc. Lond.* A **434**, 1.]

LAUFER, J. 1954 The structure of turbulence in fully developed pipe flow. *NACA Rep.* 1174.

LAWN, C. J. 1971 The determination of the rate of dissipation in turbulent pipe flow. *J. Fluid Mech.* **48**, 477.

LINDBORG, E. 1999 Correction to the four-fifths law due to variations of the dissipation. *Phys. Fluids* **11**, 510.

MANSOUR, N. N., KIM, J. & MOIN, P. 1988 Reynolds-stress and dissipation-rate budgets in a turbulent channel flow. *J. Fluid Mech.* **194**, 15 (referred to herein as MY).

MOISY, F., TABELING, P. & WILLAIME, H. 1999 Kolmogorov equation in a fully developed turbulence experiment. *Phys. Rev. Lett.* **82**, 3994.

MONIN, A. S. & YAGLOM, A. M. 1975 *Statistical Fluid Mechanics*, Vol. 2. MIT Press.

MYDLARSKI, L. & WARHAFT, Z. 1996 On the onset of high-Reynolds number grid-generated wind tunnel turbulence. *J. Fluid Mech.* **320**, 336.

NOVIKOV, E. A. 1965 Functionals and the random-force method in turbulence theory. *Sov. Phys. JETP* **20**, 1290.

QIAN, J. 1997 Inertial range and the finite Reynolds number effect of turbulence. *Phys. Rev.* E **55**, 337.

QIAN, J. 1999 Slow decay of the finite Reynolds number effect of turbulence. *Phys. Rev.* E **60**, 3409.

SADDOUGHI, S. G. 1997 Local isotropy in complex turbulent boundary layers at high Reynolds numbers. *J. Fluid Mech.* **348**, 201.

SAFFMAN, P. G. 1968 Lectures on homogeneous turbulence. In *Topics in Nonlinear Physics*, (ed. N. Zabusky), p. 485. Springer.

SREENIVASAN, K. R. 1995 On the universality of the Kolmogorov constant. *Phys. Fluids* **7**, 2778.

TOWNSEND, A. A. 1976 *The Structure of Turbulent Shear Flow*. Cambridge University Press.

ZHOU, T., ANTONIA, R. A., ZHU, Y., ORLANDI, P. & ESPOSITO, P. 1998 Performance of a transverse vorticity probe in a turbulent channel flow, *Exps. Fluids* **24**, 510.